



The effect of alignment on the electric mobility of soot

Mingdong Li, George W. Mulholland & Michael R. Zachariah

To cite this article: Mingdong Li, George W. Mulholland & Michael R. Zachariah (2016) The effect of alignment on the electric mobility of soot, *Aerosol Science and Technology*, 50:10, 1003-1016, DOI: [10.1080/02786826.2016.1213789](https://doi.org/10.1080/02786826.2016.1213789)

To link to this article: <http://dx.doi.org/10.1080/02786826.2016.1213789>

 View supplementary material 

 Accepted author version posted online: 18 Jul 2016.
Published online: 18 Jul 2016.

 Submit your article to this journal 

 Article views: 88

 View related articles 

 View Crossmark data 



The effect of alignment on the electric mobility of soot

Mingdong Li^{a,b,c}, George W. Mulholland^{a,c}, and Michael R. Zachariah^{a,b,c}

^aDepartment of Chemical and Biomolecular Engineering, University of Maryland, College Park, Maryland, USA; ^bDepartment of Chemistry and Biochemistry, University of Maryland, College Park, Maryland, USA; ^cMaterial Measurement Laboratory, National Institute of Standards and Technology, Gaithersburg, Maryland, USA

ABSTRACT

The effect of an aligning electric field on the mobility of both flame generated smoke and smolder generated smoke was studied. A pulsed differential mobility analyzer was used to study the alignment without changing the DMA flows. No detectable change in the mobility was observed for the smolder smoke, while a small but detectable effect of up to 5% decrease in the mobility diameter with increasing field was observed for the largest aggregates with a mobility diameter of 200 nm. We modeled the friction coefficient tensor of soot fractal aggregates as an equivalent prolate spheroid to obtain the field induced mobility as a function of aspect ratio. The alignment probability distribution function was determined by computing the polarizability tensor for simulated fractal aggregates. One interesting result was the smallness of the prolate sphere aspect ratio of 1.2 to 1.3 compared to the much larger aspect ratio from TEM analysis and from the polarizability ratio. An explanation for the low value based on the contribution to the friction coefficient from the individual spheres for a fractal is given. Another interesting observation is the broadening of the mobility size distribution with decreasing field. This is shown to be related to the polydispersity of the aspect ratio. The fact that all three aggregate sizes appear to fit the same spheroid aspect ratio is interesting, and offers a first-order approach to describing transport properties of aggregates. An estimate of the rotation relaxation time of the fractal aggregate was made to verify that the rotation time was much shorter than the duration of the zero electric field period during each cycle.

ARTICLE HISTORY

Received 4 September 2015
Accepted 26 April 2016

EDITOR

Christine Hrenya

1. Introduction

Most nanomaterials are not spheres (e.g., aggregates, rods, etc.), and their morphology can impact critical properties. For example, particle shape is known to be a factor in the physiochemical response in biological systems (NIOSH 2009), while transport properties are certainly particle shape dependent, including filter efficiency (Chen et al. 2013). Morphology can also greatly influence optical properties and coagulation rate (Chen et al. 1991; Weiss et al. 1992; and Colbeck et al. 1997).

A very common method employed to characterize the size of particles is mobility (Hinds 1999). By convenience, particle electrical mobility is usually expressed as an equivalent spherical diameter, (i.e., electrical mobility diameter) regardless of the actual particle shape. If one relaxes the assumption of spherical symmetry in evaluating mobility results, then one finds that mobility is dependent on the orientation of a particle relative to the

direction of its movement in an external field. This dependence opens up the possibility of characterizing shape. In previous studies, the mobility of chains, doublets of spheres, nanorods and nanotubes were demonstrated to be dependent on particle shape and particle orientation, which can be manipulated using electric fields of varying strength. Fuchs (1964) describes measurements made by Zeemann and Hoogenboom (1912) on the change in the light scattering intensity as ammonium chloride smoke was exposed to an electric field. Stöber et al. (1974) made perhaps the first conclusive measurements showing alignment of chains parallel to the electric field. Kasper and Shaw (1983) carried out an extensive study of the alignment of chain aggregates using an aerosol centrifuge, a cascade impactor, and an electrical aerosol size analyzer. By creating doublets of spheres, Kousaka et al. (1996) and Zelenyuk and Imre (2007) showed that particle orientation and thus

CONTACT Michael R. Zachariah [✉ mrz@umd.edu](mailto:mrz@umd.edu)  Material Measurement Laboratory, National Institute of Standards and Technology, 100 Bureau Dr., Mail Stop 8320, Gaithersburg, MD 20899, USA.

Color versions of one or more of the figures in the article can be found online at www.tandfonline.com/uast.

 Supplemental data for this article can be accessed on the [publisher's website](http://www.tandfonline.com/uast).

mobility is a function of electric field intensity. Song et al. (2005) demonstrated the effect of shape on particle mobility by transforming gold rods into nearly spherical particles and measuring the particle mobility diameters. They reported that the mobility diameter of the gold particles decreased from 55 nm to 25 nm. Kim et al. (2007) measured the length of carbon nanotubes by accounting for the electric field induced alignment effect. Shin et al. (2010) observed the alignment effect of 300 nm silver aggregates and reported that the mobility size increases by 20 nm from partial alignment at the higher electric field towards a random orientation at lower electric field.

In a prior work, a tensor formulation for the friction coefficient in the free molecular regime was proposed (Li et al. 2012) for computing the orientation-averaged mobility of axially symmetric particles using a Boltzmann probability distribution for the orientation. This approach was validated by experimental results of well-defined gold nanorods (Li et al. 2013). By combining both theoretical calculations and experimental measurements, both rod length and diameter were simultaneously extracted and found to be in excellent agreement with transmission electron microscope (TEM) analysis. The theory was also validated by experimental results of the doublets of NIST traceable size standard 127 nm, 150 nm, 200 nm, and 240 nm PSL spheres (Li 2012). This model, which requires information on the friction coefficient tensor, has been further extended to any particle shape in a systematic study of the mobility of non-spherical particles (Li et al. 2014a). Furthermore, to facilitate the mobility measurement at various electric field magnitudes, a new instrumental technique, employing a pulsed-field differential mobility analyzer (PFDMA), was introduced, which allows one to change the electric field acting on the particle by varying the voltage and duty cycle of a pulsed electric field (Li et al. 2014b).

In the absence of Brownian forces a non-spherical particle would align perfectly in an electric field to lower its potential energy. Brownian dynamics, however, randomize particle orientation. For sufficiently small particles over the time scales of interest, the rotational Brownian motion combined with the external electric field results in a steady-state orientation distribution—i.e., a Boltzmann angular distribution (Li et al. 2012, 2013, 2014a)—that is a function of field strength. At low electric field, the orientation of the non-spherical particle

is fully random. As the magnitude of the electric field increases, the particle is more aligned and will become fully aligned at a high electric field. The alignment process depends on the size, shape, and polarizability of the particle.

Soot generated during flaming combustion of hydrocarbon fuels is an important aerosol, though it is not easily defined either chemically or morphologically. Soot is typical of many gas-to-particle formed aerosols in that it is found in a fractal aggregate state, of many nearly uniform size spherical primary particles. Weiss et al. (1992) and Colbeck et al. (1997) have found from light scattering measurements that soot is aligned in an electric field. In this work, we study the alignment of soot aggregates through the effect of the electric field on the mobility of the aggregate particle. The mobility of soot was affected by electric field induced alignment, which results in smaller mobility diameters (i.e. higher mobility) at higher electric fields. Smoke produced by smoldering lamp wick did not show any evidence of aligning in an electric field.

2. Materials and experimental methods

A schematic of the experimental system shown in Figure 1 consists of four primary components: generation of soot and lamp wick smoke nanoparticles; size-selection with a differential mobility analyzer (DMA); particle mobility measurement at various electric fields by a pulsed-field DMA (PFDMA); and particle concentration measurement with a condensation particle counter (CPC).

2.1. Soot and lamp wick smoke generation and sampling

A Santoro style diffusion burner operating on ethylene fuel was used to generate soot particles (Santoro et al. 1983) and sampled from the flame via a sampling method described by Kim et al. (2005). Details of the soot generator and sampling were described by Ma et al. (2013). Lamp wick smoke was produced by smoldering a 25 cm length of 5 mm diameter lamp wick in a 10 L wide mouth glass jar. 5 L/min filtered air flow was directed to provide mixing within the reservoir. The burn time for one section of wick was about 20 minutes.



Figure 1. Experimental setup for soot aggregate alignment analysis.

2.2. DMA size-selection

The generated soot or lamp wick smoke particles were first passed through a Po-210 neutralizer to establish a known equilibrium charge distribution, and then to a DMA (long column, TSI Inc. Model 3081) for size selection. These experiments were conducted on DMA size-selected ~ 129 nm, ~ 154 nm and ~ 200 nm diameter soot particles, and ~ 150 nm and ~ 200 nm lamp wick smoke particles. The DMA size-selects particles at high electric fields (7200 to 7700 volts). The nominal sheath, Q_{sh} , and aerosol flows, Q_a , for the soot are 30 L/min and 0.8 L/min (125 nm), 24 L/min and 0.6 L/min (154 nm), and 16 L/min and 0.85 L/min (200 nm). The dimensionless width of the transfer function for the DMA is proportional to the ratio of the aerosol flow to the sheath flow.

2.3. PFDMA measurement

The mobility of the size-selected particles was then measured by a PFDMA at various electric fields by varying the duty cycle of a pulser system. This approach, recently described in Li et al. (2014b), employs a pulsed-square wave-field within the DMA. This allows one to change the square-wave electric field acting on the particle by changing the duty cycle of the pulse field in such a way as to maintain the same average field. For example, a square wave field of 4000 V/cm operating at a 25% duty cycle will have the same average field as a constant field of 1000 V/cm. The PFDMA can be used to measure the decrease in mobility of non-spherical particles as the electric field strength increases. This offers the potential for eventual online shape evaluation as discussed in our previous work (Li et al. 2013). The mobility measured by a PFDMA is given by (Li et al. 2014b),

$$Z_p = \frac{(Q_{sh} / D_{cycle}) \ln(r_{out} / r_{in})}{2\pi V_e L_d}, \quad [1]$$

where r_{in} is the radius of inner electrode of DMA, r_{out} is the radius of outer electrode of DMA, L_d is the 'active' length of DMA electrode, D_{cycle} is the duty cycle of the pulse (% of time that the pulse is on) and V_e is the DMA voltage.

The mobility of the size-selected soot or lamp wick smoke particles was measured in a PFDMA (long column; TSI 3081) with flow rates $Q_{sh} = 3$ L/min or $Q_{sh} = 2$ L/min and aerosol flow rates, $Q_a = 0.1$ L/min, at 100 Hz for the square wave electric pulse. These flow rates are nominal flow rates measured with a laminar flow meter with an accuracy of about 5%. The detailed experimental parameters are shown in Tables A1–A5. The mobility distributions were measured with duty

cycles ranging from 0.1 to 1 corresponding to field strength of about 8000 V/cm to 800 V/cm. All ratios of the sheath to aerosol flow exceeded 20 to guarantee suitably high resolution. To avoid the effects of time varying electric field as the particles transit the PFDMA, the PFDMA is operated in a step mode, with a step sufficiently long to ensure a complete transit through the PFDMA system before the voltage was changed (up to 45 seconds). The particles exited from the PFDMA were then counted with an ultrafine condensation particle counter (CPC) (TSI Inc. Model 3025A).

For each mobility measurement, at each duty cycle, the measurement was repeated at least three times. The assignment of DMA measurement voltage was obtained by averaging the three means of the Gaussian fits to the experimental distributions.

2.4. System calibration

The PFDMA was calibrated with NIST Standard Reference Materials (SRM) PSL spheres of 100.7 nm (SRM 1963A) on the same day under the same experimental conditions as the soot and lamp wick smoke experiments. The diluted SRM PSL 100.7 nm colloidal solution was aerosolized into the PFDMA using a 40- μ m inner diameter capillary mounted in an electrospray aerosol generator (TSI Inc. Model 3480) with a neutralizer to provide a bipolar charge distribution on the particles.

The SRM PSL mobility peak was measured and the corresponding peak diameter was determined using the Stokes—Einstein equation,

$$Z_p = qC(D_p) / (3\pi\eta D_p), \quad [2]$$

where D_p is the particle diameter, η is the gas viscosity, and $C(D_p)$ is the Cunningham slip correction. If the diameter was not equal to 100.7 μ m, then a corrected sheath flow was computed by requiring the measured mobility given by Equation (1) to result in particle diameter of 100.7 from Equation (2). This sheath flow was then used for all the PFDMA measurements for that day. More details on the PSL calibration can be found in Mulholland et al. (2006). Each duty cycle in the PFDMA measurement was then calibrated based on Equation (1) by setting the peak of the SRM PSL at 100.7 nm at this particular duty cycle with the corrected sheath flow above. The calibration process was repeated at least three times. The results of corrected and nominal sheath flow rates and calibrated and nominal duty cycles are shown in Tables A1–A5. The assignment of DMA measurement voltage for SRM PSL was obtained by averaging the three means of the Gaussian fits to the experimental profile.

2.5. TEM sample collection and analysis

Samples of the size-selected soot and lamp wick smoke were sampled by electrostatically precipitating the aerosol onto a TEM grid. The morphology and primary particle size were determined by transmission electron microscopic analysis.

3. Experimental results

In this section, experimental results on the effect of electric field on mobility are presented for the soot aggregates and the spherical lamp wick smoke. The measured results for the alignment of soot particles are then compared with our theoretical model (Li et al. 2012) where the polarizabilities are calculated using the average values of randomly formed aggregates based on the primary particle size measured by TEM. The friction coefficient tensor of the soot aggregates is modeled using an equivalent prolate spheroid in the transition regime, as the simplest non-spherical particle, and will be discussed in detail later.

The combustion generated soot or lamp wick smoke particles were first size-selected by a DMA, and then passed to the PFDMA, where particle mobility was measured at various electric fields by varying the duty cycle (Li et al. 2014b). Figure 2 shows TEM images of the DMA size-selected soot and lamp wick smoke particles. The combustion generated lamp wick smoke particles are clearly seen to be spherical, while the soot particles show an aggregate structure with primary sphere diameter ~ 10 nm. The soot aspect ratios in our TEM measurement are in the range from 1 to 3. In this case the aspect ratio is equal to the ratio of the maximum length of the aggregate divided by the projected length perpendicular to the axis

in the direction of the maximum length. For aggregates generated from a weakly sooting acetylene flame with 5 primary particles up to 164 (Samson et al. 1987), the average aspect ratio was 1.7 with a standard deviation of 0.5. The primary sphere diameters were about 30 nm and the radii of gyration ranged from 15 nm to 200 nm.

The dependence of the mobility diameter on the electric field strength for the spherical lamp wick smoke is shown in Figure 3. The mobility diameter is constant within experimental uncertainty as the field strength is increased by a factor of 7. This is the expected result because there is no preferred orientation for spherical particles. The uncertainty in these measurements, 2 nm, is about a factor of 4 larger than the soot measurements because of the time variation of the smoke generated by the smoldering lamp wick.

Due to their asymmetry, soot aggregates should align along one preferred dimension in an electric field. Therefore, partial alignment along the elongated dimension is expected as the electric field increases, which in turn should increase the observed particle mobility (decreases the observed mobility size). In Figure 4 we show that the mobility size of size-selected (~ 200 , 154 and 129 nm) soot measured is dependent on the applied electric field of the PFDMA. The variation of measured mobility diameter for the soot particles in Figure 4 shows the effect of electric field induced alignment. Higher electric fields result in more alignment, and lower drag, thus increasing mobility (decreasing mobility diameter). In Figure 4a, the size-selected ~ 200 nm soot reaches the fully aligned limit at 6000 volts/cm, but is not fully-randomly orientated even at the lowest electric field practical in our system (1069 volts/cm). The size-selected

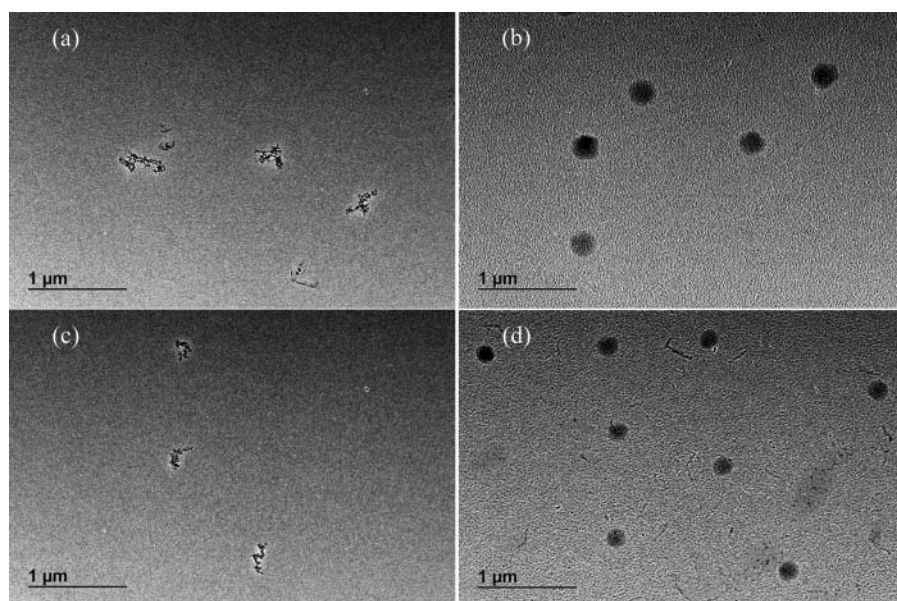


Figure 2. (a) TEM image of ~ 200 nm soot particle; (b) ~ 200 nm lamp wick smoke; (c) ~ 154 nm soot; (d) ~ 150 nm lamp wick smoke.

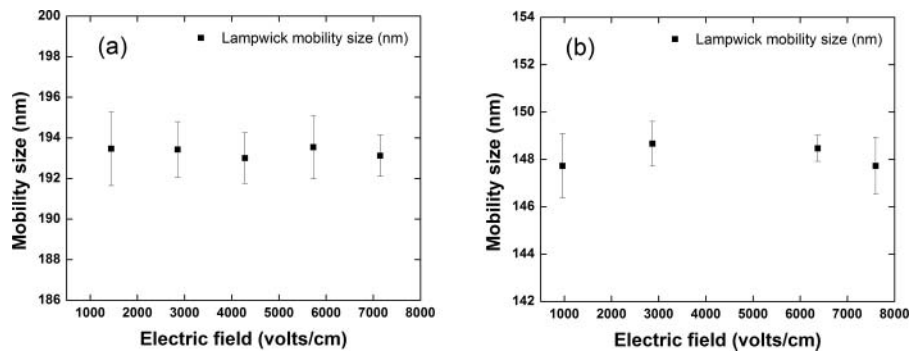


Figure 3. PFDMA measured mobility size of (a) size-selected ~ 200 nm lamp wick smoke and (b) size-selected ~ 150 nm lamp wick smoke is a constant as a function of electric field magnitude. The PFDMA was operated at sheath flow rate, $Q_{sh} = 3$ L/min ($0.5 \cdot 10^{-4}$ m³/s), and at 100 Hz. The pulse duty cycles used to obtain different electric fields for (a) and (b) are presented in Tables A1 and A2, respectively. The error bar of each data point are based on five to eight repeat voltage scans using at least two different pieces of lamp wick.

~ 154 nm soot in Figure 4b did not reach either the fully-aligned or fully-random limit in these measurements. The size-selected ~ 129 nm soot in Figure 4c appears to reach the fully random limit at low electric field 802 volts/cm, but did not reach the fully aligned limit at the 7500 volts/cm maximum operating condition for the PFDMA. In all the above three size-selected soots, the mobility diameters varied by less than 5% as the electric field was varied. The percentage changes are 4.4%, 3.9%, and 3.2% for the 200 nm, 154 nm and 129 nm soot aggregates with an uncertainty of $\pm 0.5\%$. Shin et al.

(2010) observed a similar alignment effect for 300 nm silver aggregates. They reported that the mobility size increased by 7% from partial alignment at the higher electric field, 9000 V/cm, towards a random orientation at lower electric field, 1000 V/cm.

The soot was size-selected using a DMA at a high voltage (partially aligned), and the mobility size distribution was then measured with a PFDMA at various electric fields. The mobility diameter size distribution of soot broadens when the voltage decreases (from partially aligned to randomly

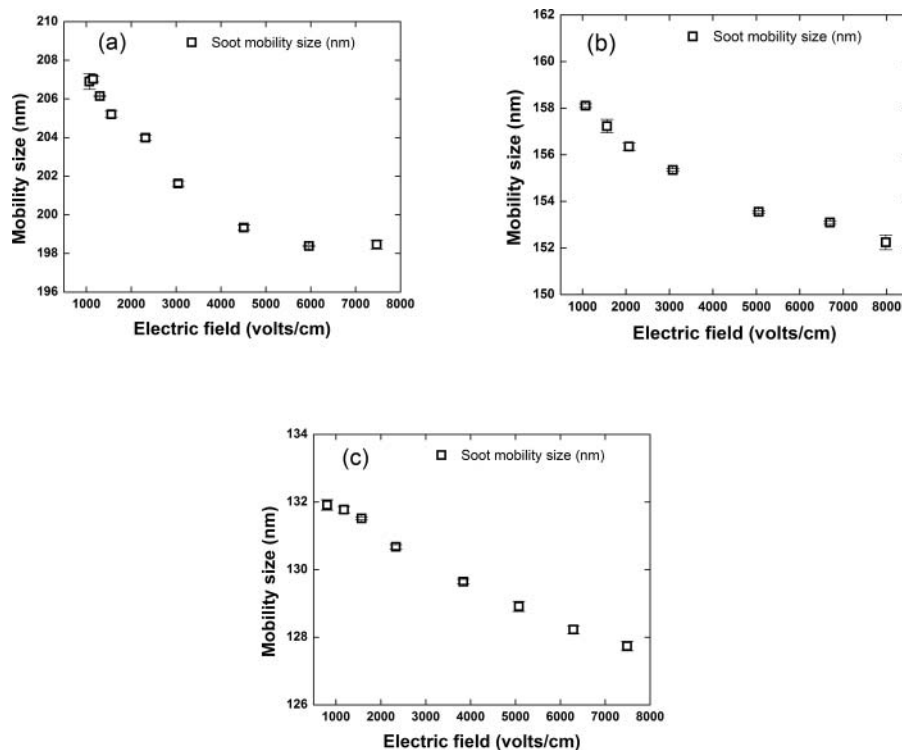


Figure 4. PFDMA measured mobility size of (a) size-selected ~ 200 nm soot and (b) size-selected ~ 154 nm soot, and (c) size-selected ~ 129 nm soot, decreases as electric field magnitude increases due to field induced alignment. The error bars of each data point are based on three repeat voltage scans.

oriented) as seen [Figures 5](#), where three plots are shown for each of the three aggregate diameters for the largest, smallest, and an intermediate voltage. These plots correspond to one curve for each electric field. The data for all eight or nine voltages is contained in the online supplementary information. The broadening effect is seen more clearly in [Figure 6](#) where the full width of the distributions at half peak concentration divided by the peak diameter (FWHP/Pk) are plotted versus the alignment voltage. The normalized width increases by 40% to 50% for the two smallest mobility diameters and by about 20% from the minimum value for the largest diameter as the voltages is decreased from 8000 V to 1000 V. The broadening of the distribution likely rises from the range of aspect ratios for the aggregates; i.e., one soot aggregate may align a lot due to a relatively larger aspect ratio, while another may not align at all due to a smaller aspect ratio close to unity, even though the two have the same high field mobility. When the electric field is decreased, the mobility diameter of the smaller aspect ratio aggregate does not change, but the mobility diameter of the larger aspect ratio aggregate becomes larger because it is less aligned. Therefore the distribution will become broader at a lower electric field. This is in part an experimental verification for the existence of alignment effect of the aggregates. Observations by [Samson et al. \(1987\)](#) of a standard deviation of the aspect ratio for soot

equal to 30% of the mean value of 1.7 are consistent with a significant variation in the aspect ratio of soot.

The normalized width of the size distributions can be compared with predicted values for the highest voltage setting. From the flow ratio of the two DMAs and the voltage setting of the DMA, one can estimate the normalized width (FWHP/Pk) for the second DMA. For the two smallest sizes, the predicted width is 0.026 compared to observed values in the range of 0.040 to 0.044. For the 200 nm aggregates, the width is 0.048 compared to a minimum observed value of 0.055. The differences between the predicted and measured values are likely due to the two DMAs not being identical and to the non-ideal performance of the DMAs, especially at the low flow ratio, 0.033, for the two smaller sizes. High resolution measurements with a flow ratio of 0.05 or less are necessary to quantify the shift in the peak diameter and the broadening of the distribution at reduced field. At a flow ratio of 0.10, the broadening effect may not be detectable.

The increase in the width for the 200 nm mobility diameter for the largest voltage is not in agreement with the expected asymptotic approach to a constant value. The deviation is likely a result of the variation of the width at fixed voltage. Seven separate measurements were made of the size distribution at the highest voltage. The mean value of the width was 0.056, which is much closer to the observed minimum of 0.055. The standard

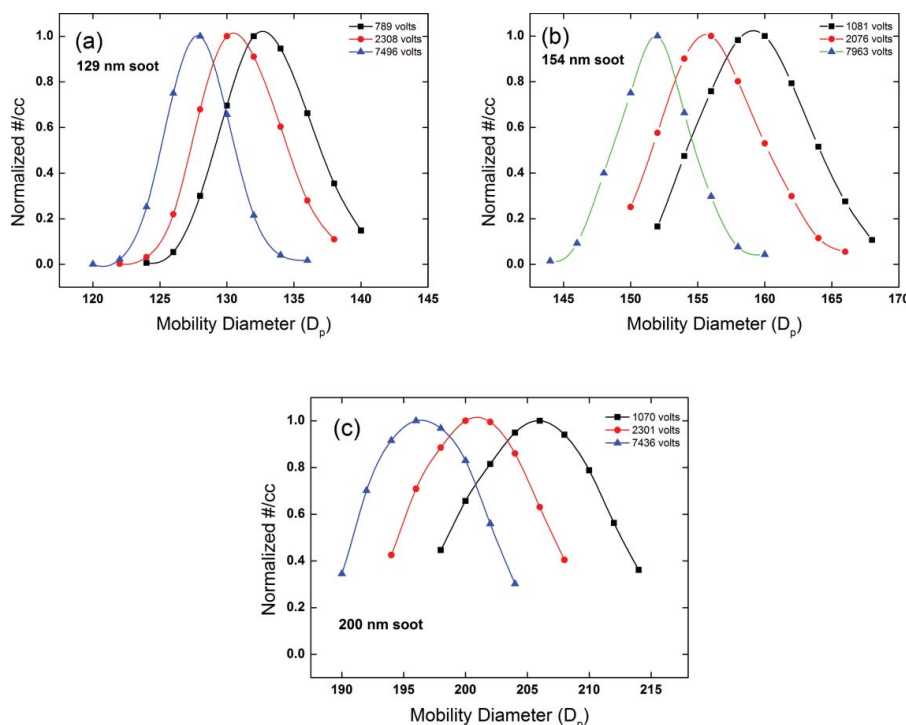


Figure 5. Normalized number concentration versus mobility diameter of (a) 129 nm, (b) 154 nm, and (c) 200 nm soot for various field strengths. The data curves are raw data without 100.7 nm PSL calibrations, which may systematically affect the peak location by 1% to 2%.

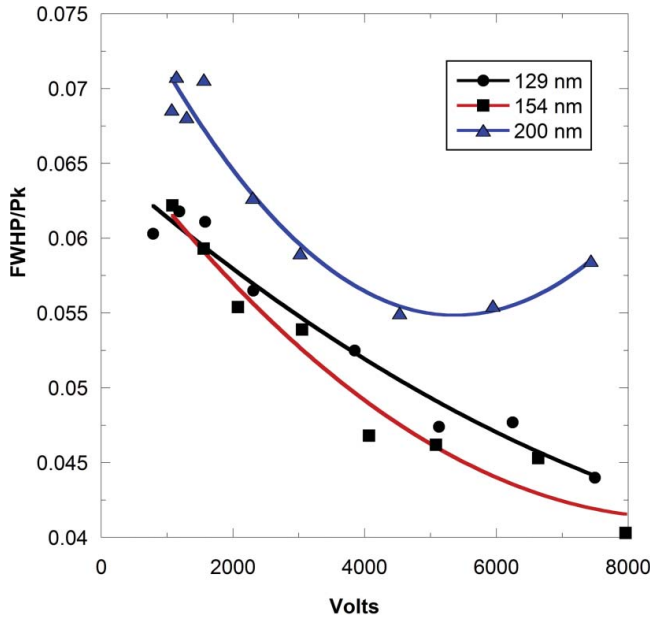


Figure 6. Full-width of mobility diameter distribution at half-peak concentration/peak diameter vs. voltage for three mobility diameters sizes.

deviation of the seven repeat measurements is 0.002. The normalized width at the highest voltage was the largest of the seven and was 1.3 standard deviations larger than the mean value. We also observe that the quadratic fits to the data in Figure 6 hint at the approach to an asymptotic width occurring at smaller voltages for larger aggregates.

4. Theory for calculating the mobility diameter as a function of electric field for soot aggregates

For a particle with arbitrary shape, the mobility as a function of the distribution of orientations was given in Li et al. (2014a, their Equation 22) by using the orientation distribution function from Fuchs (1964) and others,

$$f = \frac{e^{-U/kT}}{\int e^{-U/kT} d\Omega}, \quad [3]$$

where Ω is solid angle and U is the electric field induced energy of the conducting spheroid. This increase in the potential energy is a result of the polarization of the charge distribution from the applied electric field. In this work, to simplify the calculation, we model soot as being axi-symmetric. The purpose here is to describe soot transport as the simplest non-spherical object. For this case, the energy U is a function of the angle between the direction of the electric field and the principal axis of the prolate spheroid which is assumed to be the same as

the principle axis of the polarizability tensor. The *average electrical mobility* of an axially symmetric particle with net charge, q , in an electric field is given as (Li et al. 2012),

$$\begin{aligned} \bar{Z}_p &= q \left[K_{\perp}^{-1} + (K_{\parallel}^{-1} - K_{\perp}^{-1}) \int f \cos^2 \theta d\Omega \right] \\ &= q [K_{\perp}^{-1} + (K_{\parallel}^{-1} - K_{\perp}^{-1}) \langle \cos^2 \theta \rangle] \end{aligned} \quad [4]$$

There are two parts to Equation (4). The first part is the friction coefficient tensor, K_{\perp} and K_{\parallel} , where K_{\perp} and K_{\parallel} are the principal components of the friction coefficient tensor in the perpendicular and parallel directions (to the axial direction), respectively. The second part is the $\langle \cos^2 \theta \rangle$ term arising due to the distribution of particle orientations, which is related to particle polarizability in an electric field.

4.1. Calculating orientation, $\langle \cos^2 \theta \rangle$ for aggregates

In the presence of an electric field, a particle will be polarized which induces a torque, resulting in a tendency to align with the field if the Brownian randomization forces are not too large. The average orientation term, $\langle \cos^2 \theta \rangle$, for a particle in an electric field is determined by its polarizability (Li et al. 2013). The orientation averaged $\cos^2 \theta$ for an axisymmetric particle aggregate is given by (Li et al. 2012):

$$\langle \cos^2 \theta \rangle = \frac{1}{2\delta} \left[\frac{2\sqrt{\delta} e^{\delta}}{\sqrt{\pi} \text{Erfi}(\sqrt{\delta})} - 1 \right], \quad [5]$$

where $\delta = \frac{(\alpha_{\parallel} - \alpha_{\perp})E^2}{2kT}$, α_{\parallel} and α_{\perp} are the parallel and perpendicular components of the polarizability, E is the electric field magnitude, k is Boltzmann's constant, T is the absolute temperature, and $\text{Erfi}(z) = \frac{2}{\sqrt{\pi}} \int_0^z e^{t^2} dt$, is the imaginary error function. Thus, if the polarizability α_{\parallel} and α_{\perp} are known, $\langle \cos^2 \theta \rangle$ can be calculated. Using the primary particle size measured by TEM and the fractal parameters for soot (Sorensen 2011), we first form aggregates using computer simulation, then calculate the polarizability α_{\parallel} and α_{\perp} of those simulated aggregates. In this article the monomer number of the aggregates for a known mobility diameter was estimated using Sorensen (2011); however, an alternative method developed by Thajudeen et al. (2015a) could also have been used. This method uses regression equations derived from simulations to mimic the soot aggregation process.

Aggregates formed in combustion processes are known to be fractal-like, in which the number of

monomer spheres in the aggregate, N , scales with the aggregate radius of gyration, R_g ,

$$N = k_0 (R_g / a)^{D_f} \quad [6]$$

The quantity a is the radius of the primary sphere. Typical fractal parameters for soot are, $D_f = 1.78$ and $k_0 = 1.3$ (Sorensen 2011). Furthermore, the mobility diameter, D_m , (for a random orientation) in the transition regime has an empirical relationship with the number of monomers in the aggregate, N , via (Sorensen 2011),

$$D_m = 2a(10^{-2x+0.92})N^x, \quad [7]$$

where $x = 0.51(2\lambda / D_m)^{0.043}$, and the mean free path $\lambda = 67.3$ nm. Equation (7) is solved by iteration based on a first estimate of D_m from Equation (7) without the term $10^{-2x+0.92}$. The radius of a monomer, a , obtained from our TEM images, is ~ 5 nm. For the soot particles used in our experiments, $D_m = 200$ nm, 154 nm, and 129 nm, the corresponding number of monomers, N , was calculated to be 575, 337, and 236, respectively, based on Equation (3).

Simulated soot aggregates are generated using a cluster-cluster collision algorithm introduced by Fillippov et al. (2000) and Mackowski (2006). The basic idea is to generate a sequence of random positions, subject to the constraint that the positions at any point in the sequence satisfy Equation (6) for our target $D_f = 1.78$ and $k_0 = 1.3$. The number of monomers, N , was chosen to be 575, 337 and 236 representing $D_m = 200$ nm, 154 nm, and 129 nm soot, respectively. For each value of N , five aggregates were generated, and the eigen-values of polarizability tensor, α_1 , α_2 , and α_3 ($\alpha_1 < \alpha_2 < \alpha_3$), are calculated using the ZENO program (Mansfield et al. 2001). ZENO is a numerical calculation program for many Laplace equation boundary value problems using a random walk algorithm (Douglas et al. 1994). In the case of polarizability it assumes the particles are perfect conductors. For our purposes, ZENO has been demonstrated to be a highly accurate algorithm for computing the polarizability for an arbitrary shape (Mansfield et al. 2001). The resultant calculated eigen-values of the polarizability tensor for aggregates with $N = 575$, 337 and 236 are shown in Table 1, after averaging the values for five aggregates at constant N . The $\alpha_{||}$ and α_{\perp} needed for Equations (4) and (5) are then obtained with $\alpha_{||} = \langle \alpha_3 \rangle$ and $\alpha_{\perp} = (\langle \alpha_1 \rangle + \langle \alpha_2 \rangle) / 2$. The standard deviation of $\alpha_{||}$ is about 10% of the mean value and for α_{\perp} it is about 20%.

We have calculated the value of $\alpha_3 - (\alpha_1 + \alpha_2) / 2$, which determines the alignment effect (Equation (5)) of two aggregates with different fractal dimension. The value of $\alpha_3 - (\alpha_1 + \alpha_2) / 2$ for $k_0 = 1.3$, $D_f = 1.8$, with $N = 251$

Table 1. The $\alpha_{||}$ and α_{\perp} of soot calculated using the average values of the eigen-values of polarizability (α_1 , α_2 , α_3) of five randomly formed soot aggregates. $\alpha_{||} = \langle \alpha_3 \rangle$ and $\alpha_{\perp} = (\langle \alpha_1 \rangle + \langle \alpha_2 \rangle) / 2$.

Parameters of formed fractal aggregates	Mobility size	$\alpha_{ }$ (10^{-32} SI)	α_{\perp} (10^{-32} SI)
$N = 236$; $D_f = 1.78$; $k_0 = 1.3$; $a = 5$ nm	$D_m \sim 129$ nm	12.1	3.75
$N = 337$; $D_f = 1.78$; $k_0 = 1.3$; $a = 5$ nm	$D_m \sim 154$ nm	22.7	6.41
$N = 575$; $D_f = 1.78$; $k_0 = 1.3$; $a = 5$ nm	$D_m \sim 200$ nm	53.5	16.6

monomers is 8 times larger than the value for $k_0 = 1.3$, $D_f = 2.3$ with $N = 251$ monomers. The implication of this variation will be discussed below.

4.2. Modeling the friction coefficient tensor as an equivalent spheroid

An analytical expression for the friction coefficient tensor of an aggregate is not available in the transition regime. In this work, we assume that soot while highly ramified, can be thought of as having a major and minor axis and thus make the assumption that the friction coefficient tensor can be extracted from an equivalent prolate spheroid. The equivalent prolate spheroid has a mobility equal to that of the aggregate at the electric field of interest. This approach is similar to the equivalent sphere that is defined as a sphere that has the same mobility as a randomly oriented aggregate (zero electric field).

Dahneke's "adjusted spherical diameter" approach (Dahneke 1973) provides a way to calculate the friction coefficient of particles in the transition regime. This method has been supported by measurements for aggregates under unaligned conditions (randomly oriented) (Thajudeen et al. 2015b). We assume that the "adjusted spherical diameter" approach applies not only in situations where the aggregates show no preferential alignment, but that it applies for every orientation of the aggregate. Using Dahneke's "adjusted spherical diameter" approach (Dahneke 1973), the components of the friction coefficient of a particle in the transition regime can be expressed by the values of the friction coefficient components in the continuum regime, with an adjusted spherical diameter as (Li et al. 2013),

$$K_{||} = K_{||, \text{continuum}} / C_c(d_{a, ||})$$

and

$$K_{\perp} = K_{\perp, \text{continuum}} / C_c(d_{a, \perp}) \quad [8]$$

where the friction coefficients, $K_{||, \text{continuum}}$ and $K_{\perp, \text{continuum}}$

for a prolate spheroid in the continuum regime are given by Li et al. (2012; Equations (A7) and (A8)). The Cunningham slip correction factor

$$C_c(d_p) = 1 + \frac{2\lambda}{d_p} \left[A_1 + A_2 \exp\left(-\frac{A_3}{2\lambda/d_p}\right) \right]$$

where $A_1 = 1.142$, $A_2 = 0.558$, and $A_3 = 0.999$ for solid particles with averaged free path $\lambda = 67.3$ nm for ambient air at sea level and 23°C, are given by Allen and Raabe (1985). The adjusted diameters, $d_{a,\parallel}$ and $d_{a,\perp}$, are expressed by the friction coefficient components in the continuum regime and in the free molecular regime, $K_{\parallel, \text{freemolecular}}$ and $K_{\perp, \text{freemolecular}}$, as

$$\begin{aligned} d_{a,\parallel} &= 2\lambda(A_1 + A_2)K_{\parallel, \text{freemolecular}} / K_{\parallel, \text{continuum}} \\ d_{a,\perp} &= 2\lambda(A_1 + A_2)K_{\perp, \text{freemolecular}} / K_{\perp, \text{continuum}} \end{aligned} \quad [9]$$

($K_{\parallel, \text{freemolecular}}$ and $K_{\perp, \text{freemolecular}}$ for a prolate spheroid in the free molecular regime are given by Li et al. 2012, Equations (A3) and (A4)).

4.3. Modeling the rotational relaxation time

The model described above is based on a steady state motion of the particle; that is, it does not include the change in particle mobility when the electric field is turned on or the time for the randomization of the orientation when the field is turned off. In the study by Weiss et al. (1992), it was found that the time for soot particles to reorient as the electric field was changed from +2000 V/cm to -2000V/cm was less than the 1 ms time response for their measurements. Relaxation times for the aligned particles to randomize their motion after the field was removed ranged from 1 ms to 6 ms in the studies by Weiss et al. (1992) and by Colbeck et al. (1997) These results are for soots produced by the burning of hydrocarbon fuels. Both the size of the primary particles and the size of the clusters appear much larger than our ethene soot based on TEM images; however, there is no quantitative measure of the size distribution given.

We have estimated the time constant for randomization by computing the rotation diffusion coefficient D_{rot} in the Appendix.

$$D_{rot} = kT / (f_p N R_g^2) \quad [10]$$

where f_p is the friction coefficient of a sphere in the free molecular regime. The variance of the angle of rotation θ relative to an initial angle equal 0 is related to the

diffusion coefficient and time t by the expression:

$$\langle \theta^2 \rangle = 2D_{rot}t \quad [11]$$

We compute the rotation relaxation time as the time at which the standard deviation of the rotation angle is equal to 1 rad. This leads to the following estimate of the rotation relaxation time, τ_r :

$$\tau_r = 1 / (2D_{rot}) \quad [12]$$

For the aggregates with mobility diameters of 129 nm, 154 nm, and 200 nm, the estimated values of τ_r are 19 μ s, 40 μ s, and 125 μ s. As discussed in the Appendix, these are upper bounds to the relaxation times. Because these times are a factor of 50 or more smaller than the pulse period at zero voltage (5 ms to 8.5 ms), the effect of relaxation to random alignment on the results is negligible.

5. Comparison of experimental and predicted dependence of mobility on the electric field

The values of $\langle \cos^2 \rangle$ equal unity in the limit of fully aligned (high field strength), and 1/3 at low field strength. From these two limits one can determine K_{\perp} and K_{\parallel} from Equation (4). Using these values of K_{\perp} and K_{\parallel} together with the calculation of $\langle \cos^2 \rangle$ as a function of electric field using Equation (5), one can obtain the electric mobility as a function of field from Equation (4). Unfortunately, the experimental data is not available over a large enough range in electric field to reach the high and low field limits. Instead, the values of K_{\perp} and K_{\parallel} are estimated using Equations (8) and (9) iteratively.

We start with a guess of the aspect ratio. Using this test aspect ratio, one can obtain the two semi-axes of an equivalent prolate spheroid possessing the same mobility value as the experimentally measured mobility at a limit (fully aligned or randomly orientated). The full curve then can be drawn using the two semi-axes values based on the mobility theory of an axis-symmetric particle (Li et al. 2012) at various electric fields, and compared with the experimental data at different electric fields. For a second aspect ratio, one finds another set of semi-axes that satisfy the large field limit and from this obtains a second full curve. This process is iterated until the best fit between the theory and the experiment is obtained. Since the mobility of ~ 200 nm soot has reached the fully aligned limit at high electric field, ~ 6000 volts/cm, based on the experimental data, the size of the equivalent spheroid can be adjusted to fit the mobility value at this limit. The experimental data for ~ 200 nm soot falls between the aspect ratios of $\beta = 1.2$ and 1.3 for an

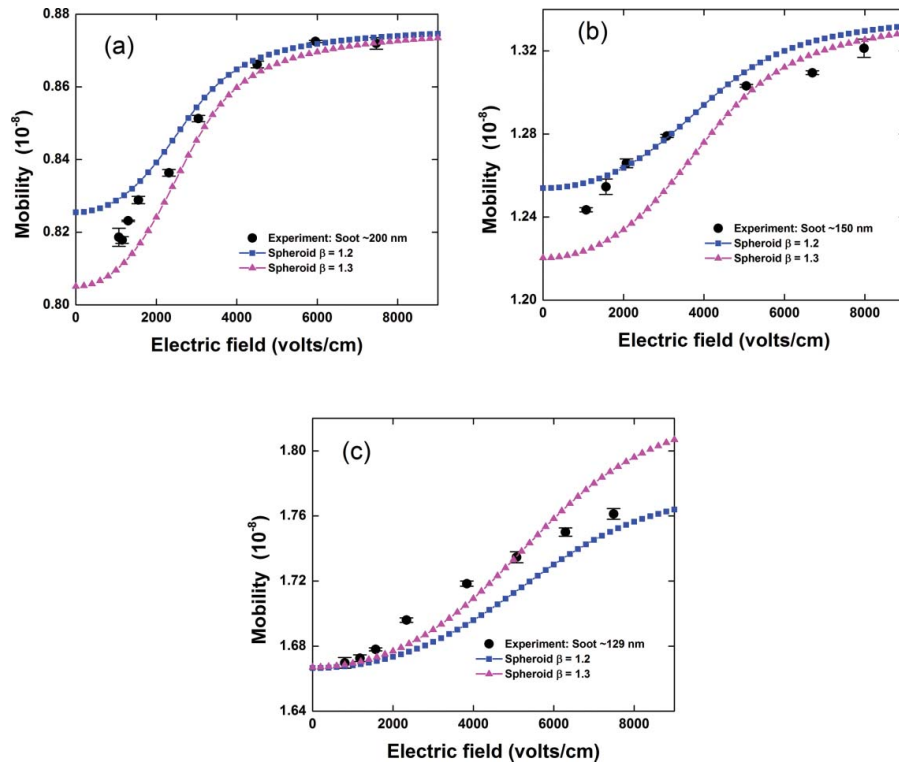


Figure 7. Experimental measured mobility for soot (black circles) (a) ~ 200 nm soot, (b) ~ 154 nm soot, and (c) ~ 129 nm soot at various applied fields. Square dotted line (blue): modeling the soot using friction coefficient tensor of an equivalent spheroid with aspect ratio $\beta = 1.2$, and using the polarizabilities from Table 1. Triangle dotted line (purple): modeling the soot using friction coefficient tensor of an equivalent spheroid with aspect ratio $\beta = 1.3$, and using the polarizabilities from Table 1.

equivalent spheroid (Figure 7a). Applying the same procedure to ~ 154 nm soot, the experimental data again roughly lie between $\beta = 1.2$ and $\beta = 1.3$ for an equivalent spheroid (Figure 7b). Since the size-selected ~ 129 nm soot approaches the fully random limit at low electric field, 802 volts/cm, we adjust the size of an equivalent spheroid to match the mobility value at the randomly oriented limit, and find two curves corresponding to aspect ratio $\beta = 1.2$ and aspect ratio $\beta = 1.3$.

6. Effect of multiply charged particles

In Figures 7b and c, the experimental data of soot show greater mobility change at the low electric fields but relatively less mobility change at high electric fields, than predicted by theory. Part of this could be a result of the wide range of aspect ratios of the aggregates together with the fact that they are ellipsoids with three unequal axes rather than prolate ellipsoids. This may also be partially due to the effect of doubly charged soot particles, which was estimated. We first fix the voltage, V , in the DMA which corresponds to size-selected D_{p1} , and count the total number of particles, N_1 , passing through the DMA and PFDMA. This experiment is repeated but with a fixed voltage $2V$, in the DMA, which corresponds to particle mobility size D_{p2} , and giving N_2 particles.

Particles with size D_{p2} but carrying double charges will be observed at size D_{p1} . The fraction of particles with actual size D_{p2} and with double charges, f , can be calculated based on a modified Boltzmann bipolar charge distribution (Wiedensohler 1988). Therefore, the fraction of doubly charged particles observed at D_{p1} is fN_2/N_1 . Our experimental results combined with the above calculation give the fractional number of doubly charged particle for $d_{p1} \sim 200$ nm, ~ 154 nm, and ~ 129 nm soot as 6%, 8.8%, and 11.6%. Those doubly charged particles with larger sizes will slightly overestimate the electric alignment effect at low electric field, but underestimate the alignment effect at high electric field. The reason is that a larger particle can contribute more mobility change at low electric field. Once it is fully aligned at a high electric field, it will make the curve more flat, which is consistent with the experimental data in Figure 7.

7. Discussion and conclusions

One noteworthy finding is that the alignment of soot aggregate's has a minor effect on the mobility diameter in the range of 5% or less for aggregates ranging in mobility size from 129 nm to 200 nm. The electrical measurements were challenging to accurately observe such a small change. Because of the smallness of the

effect, aggregate models not containing alignment may be used without large errors.

The peak separation of the mobility diameter of 7% observed by Shin et al. (2010) for silver aggregates was larger than our observed maximum of 5%. It is not known whether the difference is from the larger aggregates measured by Shin et al., 300 nm vs. 200 nm, the difference in the aggregate structure, or the difference in measurement technique of the PFTDMA versus changing the field strength by varying the flow. The aspect ratio for the silver aggregates observed by Kim et al. (2009), 1.8 ± 0.6 , is similar to the findings for soot by Samson et al. (1987), 1.7 ± 0.5 . The PFTDMA has the advantage of operating at a fixed flow ratio so that the measurement resolution is not changed as the alignment field is changed.

Even though there is a small effect on the mobility from alignment, the data in Figure 5 shows that the separation in the PFTDMA peaks could be used to qualitatively detect the presence of aggregates in an aerosol stream. For some applications where aggregates are not wanted in the production of particles, this could be of value. Initially it was hoped that the separation would be large enough to separate spherical particles from aggregates; for example, separating smolder smoke (Figure 3) from flame generated soot (Figure 4). This may not be possible because of the overlap in the distributions obtained at low and high field as shown in Figure 5.

A surprising finding from modeling the friction coefficient tensor based on a prolate spheroid is the small value of the aspect ratio, 1.2–1.3. We propose that the basic reason for the small aspect ratio is that for fractal aggregates with $D_f < 2$, the principal components of the friction coefficient tensor are approximately proportional to the number of primary particles and are thus similar in magnitude. This approach is similar to the model for aggregate mobility developed by Lall et al. (2006). One of their assumptions is the following: “Aggregates are ‘transparent’, that is, (nearly) all surfaces are directly exposed to collisions with molecules from the surrounding gas.” Even if the aggregate is twice as long in one direction as another, the friction coefficients for both orientations are expected to be similar because the structure is diffuse and almost all the primary particles will contribute to the friction coefficient for both directions.

Model calculations have shown that there is a small amount of screening in the free molecular limit (Sorensen 2011) so that the exponent x for the N dependence of the friction coefficient is slightly less than 1:

$$f_{agg} \propto N^x,$$

where x is in the range 0.92 to 0.94. So some effect of the

orientation is expected, but it would be much less than for a prolate spheroid with the same aspect ratio as the aggregate.

Two other explanations for the small aspect ratio are possible. One is that the projected areas are similar in most orientations resulting in a small aspect ratios. Previous studies have shown that the collision cross section for aggregates, which is related to the friction tensor, is related to the orientationally averaged cross section (Zang et al. 2012). Another possibility is that the polarizability eigen-vectors are not in the same direction as the friction coefficient eigen-vectors. Additional modeling is needed to resolve the cause of the small aspect ratio.

We note that equivalent prolate spheroid approximation for soot is only in terms of the friction coefficient tensor, while the polarization calculation for soot is based on simulated fractal aggregates. If the equivalent prolate spheroid approximations were made to both friction coefficient and polarization, then the theoretical curves would not fit the experimental data in Figure 7. An ideal approach would be to unify the methods either analytically or numerically for both the friction coefficient tensor of a general aggregate in the transition regime, and its polarizability tensor. A numerical model to calculate the friction coefficient of an aggregate in the transition regime, such as the one developed by Zhang et al. (2012), could be very helpful to reach an ultimate solution of the aggregate alignment theory in an electric field. Such a theory would be helpful in testing the hypothesis above about the similarity in the principal components of the friction coefficient tensor. In the meantime, the prolate sphere approximation together with experimental mobility diameter data can be useful in determining an effective aspect ratio for aggregates.

The small alignment effect of the electric field on the mobility diameter may limit the utility of this approach for determining the particle shape. Another shape parameter suggested by Heinson et al. (2010) is the quantity $A_{1,3}$, which is equal to the ratio of the square of the largest to smallest principal radii of gyration of the inertia tensor. This quantity has been shown theoretically to be related to the small angle light scattering of aggregates (Mulholland et al. 2013), and it appears to be related to the morphological shape while the friction tensor is related to the dynamic shape.

We find that changing the fractal dimension from 1.8 to 2.3 changes the polarizability factor δ in the $\langle \cos^2\theta \rangle$ expression in Equation (5) by a factor of 8. Such a large effect likely magnifies the alignment variation with respect to the aspect ratio. Unfortunately, it is not clear how one can directly measure the polarizabilities.

It is important to the development of aggregate dynamics models to perform pulsed alignment measurements on other aggregate systems to test the generality of

the observed small alignment effect and small aspect ratio for soot. Our measurements suggest a broadening of the mobility size distribution at low electric field. More detailed study of these effects with the full complement of high resolution aerosol spectrometry is warranted especially in regard to the effect of multiple charges.

Electro-optical scattering could provide complementary information on the structural aspect ratio and on the rotational diffusion coefficient. The later measurements would also be useful in testing the first-order model derived in this article for the rotational relaxation time of an aggregate.

Acknowledgments

The authors thank Dr. Jack F. Douglas and Dr. Luis Fernando Vargas Lara for providing us the ZENO program and the instructions of running ZENO. Reference to commercial equipment or supplies does not imply endorsement by the University of Maryland or the National Institute of Standards and Technology.

References

- Allen, M. D., and Raabe, O. G. (1985). Slip correction measurements of spherical solid aerosol-particles in an improved Millikan apparatus. *Aerosol Sci. Technol.*, 4:269–286.
- Chen, M. T., Xie, G. W., Yang, M., and Shaw, D. T. (1991). Experimental characterization of chain-aggregate aerosol by electrooptic scattering. *Aerosol Sci. Technol.*, 14:74–81.
- Chen, S. C., Wang, J., Fissan, H., and Pui, Y. H. D. (2013). Exposure assessment of nanosized engineered aggregates and aggregates using nuclepore filter. *J. Nanoparticle Res.*, 15:1955–1969.
- Colbeck, I., Atkinson, B., and Johart, Y. (1997). The morphology and optical properties of soot produced by different fuels. *J. Aerosol Sci.*, 28:715–723.
- Dahneke, B. E. (1973). Slip correction factors for nonspherical bodies—III the form of the general law. *J. Aerosol Med.*, 4:163–170.
- Douglas, J. F., Zhou, H.-X., and Hubbard, J. B. (1994). Hydrodynamic friction and the capacitance of arbitrarily shaped objects. *Phys. Rev. E*, 49:5319.
- Filippov, A.V., Zurita, M., and Rosner, D. E. (2000). Fractal-like aggregates: Relation between morphology and physical properties. *J. Colloid Interface Sci.*, 229:261–273.
- Fuchs, N. A. (1964). *The Mechanics of Aerosols*. Pergamon Press (distributed in the Western Hemisphere by Macmillan), Oxford, NY.
- Heinson, W. R., Sorensen, C. M., and Chakrabarti, A. (2010). Does Shape Anisotropy Control the Fractal Dimension in Diffusion-Limited Cluster-Cluster Aggregation? *Aerosol Sci. Technol.*, 44: i.
- Hinds, W. C. (1999). *Aerosol technology : properties, behavior, and measurement of airborne particles*. Wiley, New York, Chichester.
- Kasper, G., and Shaw, D.T. (1983). Comparative size distribution measurements on chain aggregates. *Aerosol Sci. Technol.*, 2:369–381.
- Kim, S. H., Fletcher, R. A., and Zachariah, M. R. (2005). Understanding the difference in oxidative properties between flame and diesel soot nanoparticles: The role of metals. *Environ. Sci. Technol.*, 39:4021–4026.
- Kim, S. H., Mulholland, G. W., and Zachariah, M. R. (2007). Understanding ion-mobility and transport properties of aerosol nanowires. *J. Aerosol Med.*, 38:823–842.
- Kim, S. C., Wang, J., Emery, M. S., Shin, W. G., Mulholland, G. W., and Pui, D. Y. H. (2009). Structural property effect of nanoparticle agglomerates on particle penetration through fibrous filters. *Aerosol Sci. Technol.*, 43:344–355.
- Kousaka, Y., Endo, Y., Ichitsubo, H., and Alonso, M. (1996). Orientation-specific dynamic shape factors for doublets and triplets of spheres in the transition regime. *Aerosol Sci. Technol.*, 24:36–44.
- Lall, A. A., Seipenbusch, M., Rong, W. Z., and Friedlander, S. K. (2006). On-line measurement of ultrafine aggregate surface area and volume distributions by electrical mobility analysis: II. Comparison of measurements and theory. *J. Aerosol Sci.*, 37:272–282.
- Li, M., Mulholland, G. W., and Zachariah, M. R. (2012). The effect of orientation on the mobility and dynamic shape factor of charged axially symmetric particles in an electric field. *Aerosol Sci. Technol.*, 46:1035–1044.
- Li, M. (2012). Quantifying particle properties from ion-mobility measurements. Chemical Physics Program. Dissertation, University of Maryland, College Park. Available online at: <http://hdl.handle.net/1903/13627>.
- Li, M., You, R., Mulholland, G. W., and Zachariah, M. R. (2013). Evaluating the mobility for gold rods in electric fields. *Aerosol Sci. Technol.*, 47:1101–1107.
- Li, M., Mulholland, G. W., and Zachariah, M. R. (2014a). Understanding the mobility of nonspherical particles in the free molecular regime. *Physical Review E*, 89:022112.
- Li, M., Mulholland, G. W., and Zachariah, M. R. (2014b). Development of a pulsed-field differential mobility analyzer: a method for measuring shape parameters for nonspherical particles. *Aerosol Sci. Technol.*, 48:22–30.
- Ma, X., Zangmeister, C. D., Gigault, J., Mulholland, G.W., and Zachariah, M. R. (2013). Soot Aggregate restructuring during water processing. *J. Aerosol Sci.*, 66:209–219.
- Mackowski, D. W. (2006). Monte Carlo simulation of hydrodynamic drag and thermophoresis of fractal aggregates of spheres in the free-molecule flow regime. *J. Aerosol Sci.*, 37:242–259.
- Mansfield, M. L., Douglas, J. F., and Garboczi, E. J. (2001). Intrinsic viscosity and the electrical polarizability of arbitrarily shaped objects. *Phys. Rev. E*, 64:061401.
- Mulholland, G. W., Donnelly, M. K., Hagwood, C. R., Kukuck, S. R., Hackley, V. A., and Pui, D. Y. H. (2006). Measurement of 100 nm and 60 nm particle standards by differential mobility analysis. *J. Res. Natl. Inst. Stand. Technol.*, 111:257–312.
- Mulholland, G. W., Lei Zhou, L., Zachariah, M. R., Heinson, W. R., Chakrabarti, A., and Sorensen, C. (2013). Light scattering shape diagnostics for nano-agglomerates. *Aerosol Sci. Technol.*, 47:520–529.
- NIOSH (2009). Approaches to safe nanotechnology: Managing the health and safety concerns associated with engineered nanomaterials: Project Report (DHHS Publication No. 2009- 125). National Institute for Occupational Safety and Health.
- Samson, R. J., Mulholland, G. W., and Gentry, J. W. (1987). Structural analysis of soot agglomerates[?]. *Langmuir*, 3:272–281.

- Santoro, R. J., Semerjian, H. G., and Dobbins, R. A. (1983). Soot particle measurements in diffusion flames. *Combustion and Flame*, 51:203–218.
- Shin, W. G., Mulholland, G. W., and Pui, D. Y. H. (2010). Determination of volume, scaling exponents, and particle alignment of nanoparticle agglomerates using tandem differential mobility analyzers. *J Aerosol Sci.*, 41:665–681.
- Song, D. K., Lenggono, I. W., Hayashi, Y., Okuyama, K., and Kim, S. S. (2005). Changes in the shape and mobility of colloidal gold nanorods with electrospray and differential mobility analyzer methods. *Langmuir*, 21:10375–10382.
- Sorensen, C. M. (2011). The mobility of fractal aggregates: a review. *Aerosol Sci. Technol.*, 45:765–779.
- Stöber, W., Boose, C., and Prodi, V. (1974). Über die Orientierung und den dynamischen Formfaktor von kettenförmigen Aerosolteilchen in Ladungsspektrometern. *Water, Air and Soil Pollution*, 3:493.
- Thajudeen, T., Deshmukh, S., and Hogan, C. J. (2015a). Langevin simulation of aggregate formation in the transition regime. *Aerosol Sci. Tech.*, 49:115–125.
- Thajudeen, T., Jeon, S., and Hogan, C. J. (2015b). The mobilities of flame synthesized aggregates/agglomerates in the transition regime. *J. Aerosol Sci.*, 80:45–57.
- Weiss, R. E., Kapustin, V. N., and Hobbs, P. V. (1992). Chain-aggregate aerosols in smoke from the Kuwait oil fires. *J. Geophys. Res.*, 97:14527–14531.
- Wiedensohler, A. (1988). An approximation of the bipolar charge distribution for particles in the submicron size range. *J. Aerosol Sci.*, 19:387–389.
- Zeemann, P., and Hoogenboom, C. (1912). Electric double refraction in some artificial clouds and vapors. *Phys. Z.*, 13:913–920.
- Zelenyuk, A., and Imre, D. (2007). On the effect of particle alignment in the DMA. *Aerosol Sci Tech.*, 41:112–124.
- Zhang, C., Thajudeen, T., Larriba, C., Schwartzentruber, T. E., and Hogan, C. J. (2012). Determination of the scalar friction factor for non-spherical particles and aggregates across the entire Knudsen number range by direct simulation Monte Carlo (DSMC). *Aerosol Sci Tech.*, 46:1065–1078.

Appendix

An estimate of the diffusion coefficient of an aggregate in the free molecular regime is derived for estimating the rotational relaxation time. We assume that the friction force on the i th primary sphere, F_p , in an aggregate is equal to the friction coefficient of the primary sphere (Friedlander), f_p , times the velocity of the sphere as it rotates into motionless ambient air about the center of mass.

$$\vec{F}_p = f_p \vec{v} = f_p \vec{v}_r(i) = f_p \omega \vec{n}_r(i), \quad [A1]$$

where $\vec{n}_r(i)$ is the unit vector perpendicular to \vec{r}_i , the coordinate of the i th particle projected on the x, y plane relative to the center of mass, and ω is the constant rotation velocity about the minor principal axes (z). The friction

Table A1. Summary of the calibrated sheath flow rate and pulse duty cycles for PFDMA measurements to size-selected ~200 nm lamp wick smoke at 100 Hz. Those calibrations were based on 100.7 nm NIST standard reference material (PSL sphere) measured in three repeat voltage scans under the same experimental conditions as the lamp wick smoke measurements on the same day.

Nominal sheath flow rate	3 L/min					
Calibrated sheath flow rate	2.97 L/min					
Nominal pulse duty cycle	0.2	0.25	0.333	0.5	1 (DC)	
Calibrated pulse duty cycle	0.202	0.252	0.336	0.506	1 (DC)	

Table A2. Summary of the calibrated sheath flow rate and pulse duty cycles for PFDMA measurements to size-selected ~150 nm lamp wick smoke at 100 Hz. Those calibrations were based on 100.7 nm NIST standard reference material (PSL sphere) measured in three repeat voltage scans under the same experimental conditions as the lamp wick smoke measurements on the same day.

Nominal sheath flow rate	3 L/min					
Calibrated sheath flow rate	3.02 L/min					
Nominal pulse duty cycle	0.125	0.15	0.333	1 (DC)		
Calibrated pulse duty cycle	0.126	0.152	0.338	1 (DC)		

Table A3. Summary of the calibrated sheath flow rate and pulse duty cycles for PFDMA measurements to size-selected ~200 nm soot at 100 Hz. Those calibrations were based on 100.7 nm NIST standard reference material (PSL sphere) measured in three repeat voltage scans under the same experimental conditions as the soot measurements on the same day.

Nominal sheath flow rate	2 L/min								
Calibrated sheath flow rate	1.98 L/min								
Nominal pulse duty cycle	0.133	0.167	0.222	0.333	0.444	0.667	0.8	0.909	1 (DC)
Calibrated pulse duty cycle	0.134	0.168	0.224	0.337	0.452	0.680	0.816	0.931	1 (DC)

Table A4. Summary of the calibrated sheath flow rate and pulse duty cycles for PFDMA measurements to size-selected ~150 nm soot at 100 Hz. Those calibrations were based on 100.7 nm NIST standard reference material (PSL sphere) measured in three repeat voltage scans under the same experimental conditions as the soot measurements on the same day.

Nominal sheath flow rate	3 L/min								
Calibrated sheath flow rate	3.02 L/min								
Nominal pulse duty cycle	0.125	0.15	0.2	0.25	0.333	0.5	0.667	1 (DC)	
Calibrated pulse duty cycle	0.126	0.152	0.202	0.253	0.338	0.508	0.680	1 (DC)	

Table A5. Summary of the calibrated sheath flow rate and pulse duty cycles for PFDMA measurements to size-selected ~ 125 nm soot at 100 Hz. Those calibrations were based on 100.7 nm NIST standard reference material (PSL sphere) measured in three repeat voltage scans under the same experimental conditions as the soot measurements on the same day.

Nominal sheath flow rate	3 L/min							
Calibrated sheath flow rate	3.03 L/min							
Nominal pulse duty cycle	0.1	0.12	0.15	0.2	0.333	0.5	0.667	1 (DC)
Calibrated pulse duty cycle	0.101	0.122	0.152	0.203	0.338	0.508	0.680	1 (DC)

coefficient for the primary sphere is given by

$$f_p = \frac{2}{3} d_p^3 \rho \left(\frac{2\pi kT}{m} \right)^{1/2} \left[1 + \frac{\pi\alpha}{8} \right], \quad [\text{A2}]$$

where d_p is the particle diameter, ρ is the gas density, m the molecular mass of the gas molecules (assumed to be nitrogen), and α the momentum accommodation coefficient taken to be 0.9.

The torque acting on this i th particle, Γ_i , reduces to the following simple form because the radius vector and

the unit normal vectors are perpendicular;

$$\Gamma_i = \vec{r}_i \times F p_i = f_p \omega r_i^2 \quad [\text{A3}]$$

The total torque resistance, Γ , is obtained by summing over all primary spheres.

$$\Gamma = f_p \omega \sum_1^N r_i^2 = f_p \omega N R_{g1}^2, \quad [\text{A4}]$$

where the radius of gyration, R_{g1} , is relative to the minor principal axes (maximum torque). The torque resistance coefficient, γ_c , is the factor multiplying the angular velocity in Equation (A4). The rotational diffusion coefficient, D_{rot} is related to γ_c by the following equation:

$$D_{rot} = kT / \gamma_c = kT / (f_p N R_{g1}^2) \approx kT / (f_p N R_g^2) \quad [\text{A5}]$$

The expression on the right hand side underestimates the diffusion coefficient because the radius of gyration is larger than the projected radius of gyration. For an aspect ratio of 1.7, the underestimate is about 25%. The diffusion coefficient is also underestimated because the friction coefficient per particle, f_p , is about a factor two larger than the value determined from the measured mobility diameter of the aggregates because of screening in the actual aggregate. Our expression provides a lower bound to the aggregate diffusion coefficient.